Anal. Chem. **2008,** *80,* 2244−2249

Gold Nanohole Array Substrates as Immunobiosensors

John C. Sharpe,*,† John S. Mitchell,† Ling Lin,‡ Nemanya Sedoglavich,§ and Richard J. Blaikie‡

The Horticulture and Food Research Institute of New Zealand, East Street, Private Bag 3123, Hamilton 3240, New Zealand, MacDiarmid Institute for Advanced Materials and Nanotechnology, Department of Electrical and Computer Engineering, University of Canterbury, Private Bag 4800, Christchurch 8020, New Zealand, and Department of Engineering, University of Waikato, Private Bag 3015, Hamilton 3240, New Zealand

A gold nanohole array is functionalized with a cortisol thiol derivative, and binding to a monoclonal antibody is conveniently detected using the sensitive shift in the 1060 nm transmission peak of the array. Detection is also enhanced 3-fold by the application of a secondary antibody−gold nanoparticle conjugate. This regenerable response represents a more sensitive shift than that obtained previously for higher affinity binding and opens the way to application of nanohole arrays in immunobiosensing of important biomolecules.

Since the first reported observation of extraordinary optical transmission through subwavelength noble metallic film nanohole arrays,[1] there has been much interest in predicting and studying the behavior of light interactions with such structures.[2−11] Where charge cloud effects operate near noble metal surfaces, plasmonic mechanisms in particular lead to unique phenomena including photon-electron energy transfer. It has been shown[2] that surface plasmon polaritons (SPPs), as well as localized surface plasmons (LSPs), dominate the spectral transmission signature for such periodic nanohole structures over a range of hole grid periods. Recent advances in fabrication techniques such as electron beam lithography (EBL), focused ion beam (FIB) lithography, and soft lithography have provided the necessary precision to build nanoscale planar devices with highly defined features. Nanohole array devices have been fabricated to explore effects on light transmission with varying dielectric constant of the adjacent medium,[3] hole diameter,[4] geometry,[5] film thickness,[6] polarization, orientation and aspect ratio,[7] and multiple layers.[8] Single-hole studies have been performed and contrasted with multihole arrays.[9] Plasmonic metamaterials have been produced to explore quasi-infinite nanohole array interactions.[10] The mechanisms involved in enhanced transmission of many of these devices have also been modeled theoretically.[11,12]

Much of this work to date shows significant promise for industrial application of nanohole array devices in fields ranging from semiconductor components to medical devices. In particular, there is strong demand for sensitive and robust transduction elements for biosensors. Surface plasmon resonance (SPR) instrumentation is becoming commonplace in many research laboratories as a means to observe and measure biochemical interactions in real time.[13,14] However, while high sensitivity can be achieved with these systems, the mechanical and temperature stability requirements for making reliable measurements with these devices heavily limit their application to laboratory environments. Further miniaturization, cost reduction, and alternative approaches will be required if SPR type devices are to reach point-of-care or field applications.

Several devices have been developed that require simpler instrumentation such as low cost CCD spectrometers that promise to provide a pathway for low-cost field use biosensor systems using localized surface plasmon resonance (LSPR) effects.[15,16] One example of this approach is to use nanosphere lithography to create uniform arrays of surface-bound particles that are highly sensitive to their immediate surrounding dielectric environment.[17]

Nanohole-based systems have also been studied with specific regard to biosensor devices.[18−20] Potential advantages of using

* To whom correspondence should be addressed. E-mail: jsharpe@hortresearch.co.nz. Fax: +64 7 858 4700.

† The Horticulture and Food Research Institute of New Zealand.

‡ University of Canterbury.

§ University of Waikato.

(1) Ebbesen, T. W.; Lezec, H. J.; Ghaemi, H. F.; Thio, T.; Wolff, P. A. *Nature* **1998**, *391*, 667−669.

(2) Krishnan, A.; Thio, T.; Kima, T. J.; Lezec, H. J.; Ebbesen, T. W.; Wolff, P. A.; Pendry, J.; Martin-Moreno, L.; Garcia-Vidal, F. J. *Opt. Commun.* **2001**, *200*, 1−6.

(3) Degiron, A.; Ebbesen, T. W. *J. Opt. A: Pure Appl. Opt.* **2005**, *7*, S90−S96.

(4) Prikulis, J.; Hanarp, P.; Olofsson, L.; Sutherland, D.; Kall, M. *Nano Lett.* **2004**, *4*, 1003−1007.

(5) Baida, F. I.; Van Labeke, D. *Opt. Commun.* **2002**, *209*, 17−22.

(6) Kim, J. H.; Moyer, P. J. *Opt. Express* **2006**, *14*, 6595−6603.

(7) Gordon, R.; Brolo, A. G.; McKinnon, A.; Rajora, A.; Leathem, B.; Kavanagh, K. L. *Phys. Rev. Lett.* **2004**, *9203*, 7401−7404.

(8) Lin, L.; Reeves, R. J.; Blaikie, R. J. *Phys. Rev. B* **2006**, *74*, 155407.

(9) Rindzevicius, T.; Alaverdyan, Y.; Dahlin, A.; Hook, F.; Sutherland, D. S.; Kall, M. *Nano Lett.* **2005**, *5*, 2335−2339.

(10) Henzie, J.; Lee, M. H.; Odom, T. W. *Nat. Nanotechnol.* **2007**, *2*, 549−559.

(11) Chang, S. H.; Gray, S. K.; Schatz, G. C. *Opt. Express* **2005**, *13*, 3150−3165.

(12) Chen, Y. G.; Wang, Y. H.; Zhang, Y.; Lu, S. T. *Opt. Commun.* **2007**, *274*, 236−240.

(13) Karlsson, R. *J. Mol. Recognit.* **2004**, *17*, 151−161.

(14) Mitchell, J. S.; Wu, Y.; Cook, C. J.; Main, L. *Bioconjugate Chem.* **2007**, *18*, 268−274.

(15) Haes, A. J.; Van Duyne, R. P. *Anal. Bioanal. Chem.* **2004**, *379*, 920−930.

(16) Willets, K. A.; Van Duyne, R. P. *Annu. Rev. Phys. Chem.* **2007**, *58*, 267−297.

(17) Haynes, C. L.; Van Duyne, R. P. *J. Phys. Chem. B* **2001**, *105*, 5599−5611.

(18) Brolo, A. G.; Gordon, R.; Leathem, B.; Kavanagh, K. L. *Langmuir* **2004**, *20*, 4813−4815.

(19) Gao, D.; Chen, W.; Mulchandani, A.; Schultz, J. S. *Appl. Phys. Lett.* **2007**, *90*, 073901.

(20) De Leebeeck, A.; Kumar, L. K. S.; de Lange, V.; Sinton, D.; Gordon, R.; Brolo, A. G. *Anal. Chem.* **2007**, *70*, 4094−4100.

10.1021/ac702555r CCC: $40.75
Published on Web 02/21/2008

nanohole array films over the analogous monodisperse arrangement of arrays of discrete surface-bound metal nanoparticles include a reduced active functionalization area and therefore increased sensitivity, simplified optical setup using transmission measurement with well-defined spectral features rather than broad peak absorption, and optical field concentration and therefore enhancement effects. Previous work has investigated and measured elastic scattering during binding interactions and compared these indented nanohole systems with equivalent projected geometry elements.[4] Nanohole features have also been utilized to enhance fluorescent label excitation[21−23] and radiative decay rates in single molecule studies[24] and in Raman scattering[25] work.

In this report, we explore several facets of nanohole array performance with sensing applications in mind. Transmission characteristics of nanohole arrays are studied for the hole grid period and varying dielectric constants. We report the immobilization of a novel cortisol thiol conjugate to the surface of a gold nanohole array, with the binding of this conjugate to a monoclonal antibody and a further secondary antibody or antibody−gold signal enhancement agent to determine likely biosensing performance. To our knowledge, this is the first report of the use of a discrete steroid−linker−thiol derivative for immobilization on a gold surface, an immunochemical interaction monitored using nanohole arrays, and the use of gold nanoparticles to enhance binding response from an antibody on a nanohole array. This regenerable system is also studied for consistent multisample binding response.

EXPERIMENTAL METHOD AND MATERIALS

Fabrication of Nanohole Array Substrates. Figure 1a shows the schematic of the structure used in this study. The Au nanohole arrays were prepared on a BK7 glass substrate (microscope cover slips 22 mm × 22 mm × 0.20 mm). After solvent (acetone, methanol, and IPA) cleaning, a layer of poly(methyl methacrylate) (PMMA) was spun onto the substrate. A nanodot-array pattern was then defined onto the PMMA by means of electron beam lithography (EBL). Next, the EBL-exposed PMMA was removed with a solution of methyl isobutyl ketone (MIBK) in isopropyl alcohol (IPA). Thereafter, a layer of 5 nm thick NiCr followed by a layer of 40 nm thick Au were thermally evaporated onto the sample (rate, 2 nm s^{-1}; process pressure, 2×10^{-3} mbar). The purpose of the NiCr layer was to improve the adhesiveness of Au onto the substrate. Subsequently, Au nanohole arrays were created on the substrate through the removal of the PMMA nanodots via a solvent-assisted lift-off process. A SEM image of a fabricated Au nanohole array is shown in Figure 1b. We fabricated a series of 1.0 mm × 1.0 mm Au nanohole array patterns on each individual coverslip, on which the periods of the nanohole array, *P*, ranged from 500 to 600 nm with an increment of 20 nm, and the diameter of the holes, *D*, varied from 70 to 200 nm. Up to nine discrete regions (with a particular hole and period geometry) were produced on each coverslip.

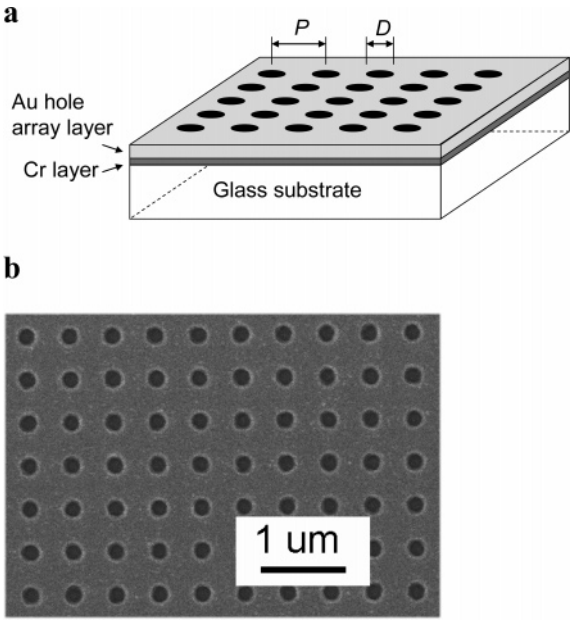

Figure 1. (a) Schematic diagram of the structure studied, showing gold hole array layer with period, *P*, and hole diameter, *D*. (b) SEM image of a fabricated substrate showing Au film through-holes on a glass substrate.

Transmission-Mode Spectrophotometry of Mounted Substrate. Optical transmission measurements were performed on the nanohole array substrates using a modified Shimadzu 1605 dual beam spectrophotometer. The optical path was modified by replacing the standard sample holders with a precisely machined aperture (0.70 mm in diameter) and flow cell platform as shown in Figure 2a. The flow cell was custom designed and manufactured using 3D photocure printing techniques and materials (R11 Perfactory Resin, StrataTec, Christchurch, New Zealand) to provide a 30 μL laminar flow volume (internal dimensions of the flow channel were 20 mm × 1.5 mm × 1 mm, Figure 2b) for multiple array regions. The nanohole array substrate was mounted to one side of the flow cell with a second microscope slide sealing the flow chamber while allowing light transmission. A white light source was projected onto the nanohole array, and transmission was measured over a wavelength range from 400 to 1100 nm. Sample and buffer flow was controlled using a peristaltic pump (P625/900.133, Instech Laboratories, Plymouth Meeting, PA) operated in suction mode with air bubble spacers used to avoid cross contamination between samples and buffer reagents. The running buffer used was HEPES buffered saline (HBS-EP, 0.01 M, 0.15 M NaCl) with EDTA (3 mM) and 0.005% Tween-20 detergent. Unless otherwise stated, binding procedures were conducted at a constant flow rate of 5.5 μL min^{-1} with an increased rate of 140 μL min^{-1} for buffer flushes and purges. For temperature studies, the flow cell volume temperature was controlled using a resistive heater element attached to the glass slide to provide a good thermal conduction path. During these tests, flow was stopped and sufficient time (5 min) was given to allow the flow cell, fluid, and array to reach thermal equilibrium before acquiring spectral transmission data. Aqueous sucrose solutions were prepared to provide the desired bulk refractive index over

(21) Liu, Y. D.; Blair, S. *Opt. Lett.* **2003**, *28*, 507−509.
(22) Brolo, A. G.; Kwok, S. C.; Moffitt, M. G.; Gordon, R.; Riordon, J.; Kavanagh, K. L. *J. Am. Chem. Soc.* **2005**, *127*, 14936−14941.
(23) Brolo, A. G.; Kwok, S. C.; Cooper, M. D.; Moffitt, M. G.; Wang, C. W.; Gordon, R.; Riordon, J.; Kavanagh, K. L. *J. Phys. Chem. B* **2006**, *110*, 8307−8313.
(24) Wenger, J.; Lenne, P. F.; Popov, E.; Rigneault, H.; Dintinger, J.; Ebbesen, T. W. *Opt. Express* **2005**, *13*, 7035−7044.
(25) Brolo, A. G.; Arctander, E.; Gordon, R.; Leathem, B.; Kavanagh, K. L. *Nano Lett.* **2004**, *4*, 2015−2018.

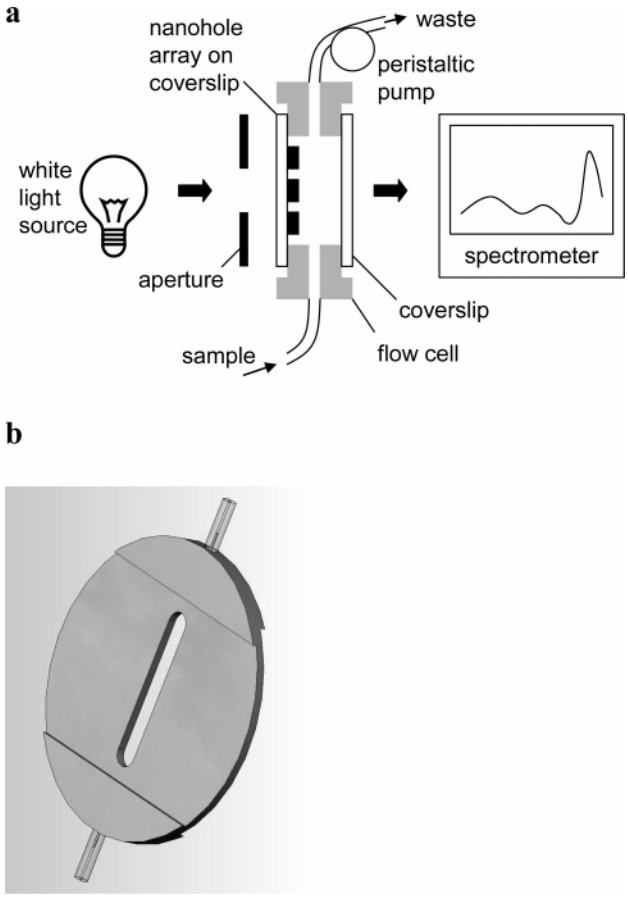

Figure 2. (a) Schematic diagram of measurement system showing light source, fluid path, and light transmission to spectrometer. (b) Flow cell with 30 μL internal volume (internal channel length = 20 mm).

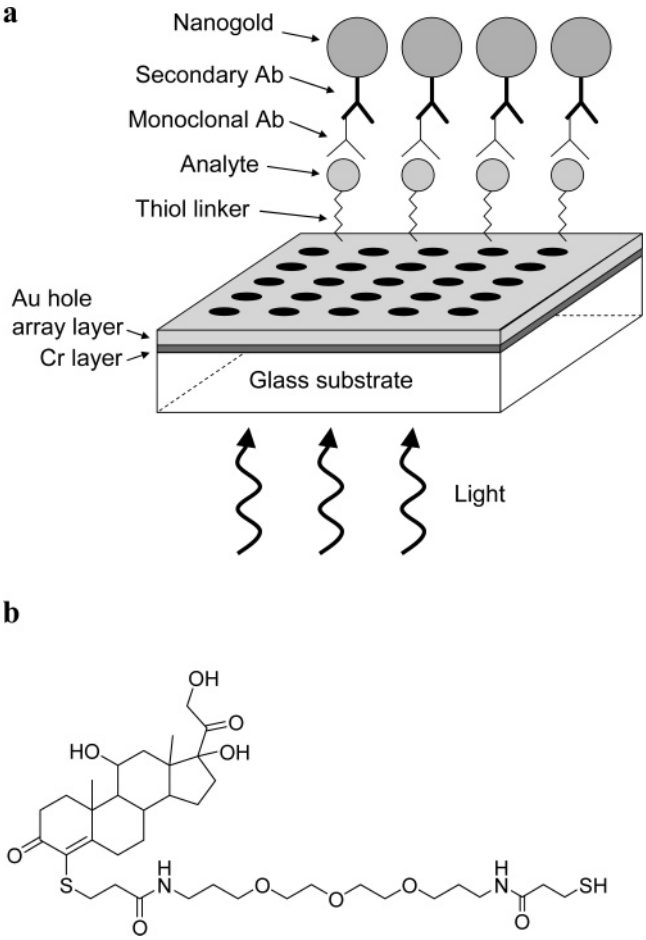

Figure 3. (a) Binding schematic for gold nanohole surface immobilized with cortisol-OEG-SH analyte, bound monoclonal, and secondary antibody-gold and (b) structure of cortisol-OEG-SH.

a range of values from 0% to 50% w/v (0, 1, 2, 5, 10, 20, 35, 50%) corresponding to a range of $n = 1.3330$ to $n = 1.4201$. When performing bulk refractive index measurements, sucrose solutions were measured at random to ensure objective data.

Antibody Binding Tests. Each injection was preceded and followed by a small air bubble to prevent mixing with the buffer stream. This was followed by either anti-mouse IgG secondary antibody−gold 40 nm diameter conjugate (BA.GAM 40, British Biocell, Cardiff, U.K.) (2 × 25 μL undiluted) or anti-mouse IgG secondary antibody (M7023, Sigma, St, Louis, MO, 2 × 25 μL, 400 μg mL^{-1}). All spectral peak shifts stated were after the flow cell had been returned to running buffer. All experiments used HEPES-buffered saline with EDTA and Tween 20 pH 7.4 (HBS-EP) running buffer. Four replicates of each binding were performed. Nonspecific binding tests for both secondary antibody−gold and secondary antibody were performed by injecting the secondary antibody (2 × 25 μL at the above concentrations) without first injecting primary antibody. All surfaces were regenerated with 20 mM NaOH (2 × 25 μL injections). A schematic depiction of the final bound conjugate thiol−cortisol−mAb−IgG−gold system is shown in Figure 3a.

RESULTS AND DISCUSSION

Immobilization of Nanohole Array Surface with Cortisol and Antibody Binding Interactions. The nanohole array substrate was first cleaned with absolute ethanol (six rinses) and was air-dried. An ethanolic solution of cortisol-OEG-SH (Figure 3b) (5 μL, 10 mg mL^{-1}) was applied to the gold nanoarray surface, incubated at room temperature for 16 h in the dark, and allowed to evaporate. Additional 5 μL volumes were applied twice for a further 5 h each. The slide was then rinsed with ethanol and mounted and bound into the flow cell. To ensure saturation of immobilized analyte on the mounted substrate surface, a further ethanolic solution of cortisol-OEG-SH (100 μL, 1 mg mL^{-1}) was flowed over the flow cell in situ and allowed to pass through over a 1 h period. The surface was then rinsed with water before running HBS-EP buffer. There was a 5.5 nm red shift of the maximum transmission peak upon in situ immobilization. For synthesis of the cortisol-OEG-SH compound, please see Supporting Information. Monoclonal anti-cortisol (US Biologicals, C7904-11B) was passed over the surfaces (10 μg mL^{-1}, 2 × 25 μL) with each pulse separated by a buffer rinse into the flow cell.

Transmission Spectra, Response, and Substrate Selection. There are two main plasmon modes that lend nanohole array devices to sensing applications: LSPR effects of single holes (top and bottom interface) in the array film and surface plasmon polaritons (SPPs) that result from the periodicity of the structure.[1,2] Figure 4 illustrates the in-air nanohole array transmission response to hole period from $P = 500$ to 600 nm in 20 nm increments. Features to note include a broad transmission peak centered at

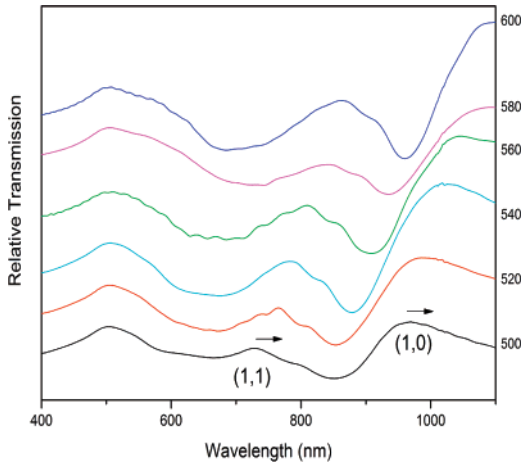

Figure 4. Transmission spectra for nanohole array periods P = 500 (black), 520 (red), 540 (blue-green), 560 (green), 580 (pink), 600 (blue). Spectra are offset vertically from the P = 500 nm curve for clarity. SPP resonance peaks (1,1) and (1,0) are observed to shift red with increased hole spacing.

510 nm due to general light transmission of the relatively thin 40 nm gold layer used[6] and between 700 and 1100 nm two additional peaks that can be attributed to plasmonic effects. The nanohole arrays support enhanced transmission at wavelengths that match the SPP resonance condition. The approximate position of these peaks can be determined by the equation[26]

$$\lambda_{max}(i,j) = \frac{P}{\sqrt{\frac{4}{3}(i^2 + ij + j^2)}}\sqrt{\frac{\epsilon_1\epsilon_2}{\epsilon_1 + \epsilon_2}} \qquad (1)$$

where P is the hole grid period, integers i and j are the scattering orders from the array, and ϵ_1 and ϵ_2 are the dielectric constants of the metal and the surrounding dielectric medium, respectively. From this relationship, it can be seen that the SPP resonances depend on hole spacing and dielectric properties of the interface. Equation 1 tends to predict resonance peak positions that are lower than those achieved experimentally because interactions between LSPR and SPPs are neglected, even though the spectral positions of the transmission peaks are dominated by the SPP modes.[3,8] Simulations performed using FDTD Solutions software (Lumerical Solutions, Inc. Vancouver, Canada) also produced an envelope with similar features but with blue-shifted peaks relative to experimental findings. Nevertheless, in accordance with this equation, the first $\lambda_{max}(i,j)$ = (1,1) SPP resonance peak undergoes a red shift from 737 to 873 nm with increasing hole spacing, while a second (1,0) peak shifts from 977 nm to over 1100 nm.

An array period of 520 nm was chosen for our refractive index and binding studies. This period was chosen in a tradeoff between the transmission curve profile (peak to trough ratio), the dynamic range of the spectrometer, and our ability to resolve red-shifted (1,0) peaks. A hole diameter of 150 nm was chosen for our studies where hole uniformity and transmission efficiency provided well-defined transmission peaks.

Spectral Response to Change in Bulk Refractive Index. By introduction of a number of solutions, it is possible to determine the approximate sensitivity to the bulk refractive index to within approximately 6−10 nm[16] of the nanohole array substrate surface. SPR extends out to around 200−300 nm[27] from a planar gold surface. Figure 5a shows a typical transmission spectra for one of the substrate regions (P = 520 nm) studied in the presence of air and buffer solution (HBS). Sucrose solutions (0% to 50% w/v corresponding to a range of 1.33−1.42) were also introduced to the nanohole array surface via the flow cell. Figure 5b shows the relative response in terms of the transmission peak shift for the (1,0) transmission peak over this refractive index range for a nanohole array substrate region with the P = 520 nm nanohole array region. It was found that the response of this peak to the refractive index was greater than the (1,1) peak, with this reduced sensitivity likely to be due to superposition of this transmission feature with the broad 510 nm transmission of the gold film in addition to other plasmon modes. Previous reports[20] have studied spectral response over lesser refractive index ranges (1.33−1.36). Here we examine an extended range (to 1.42) and find a nonlinear spectral response. This relationship has not previously been reported experimentally; however, eq 1 does predict such an effect.

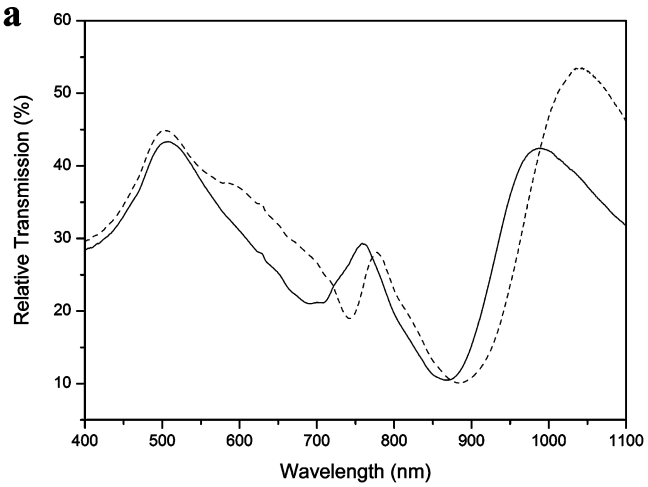

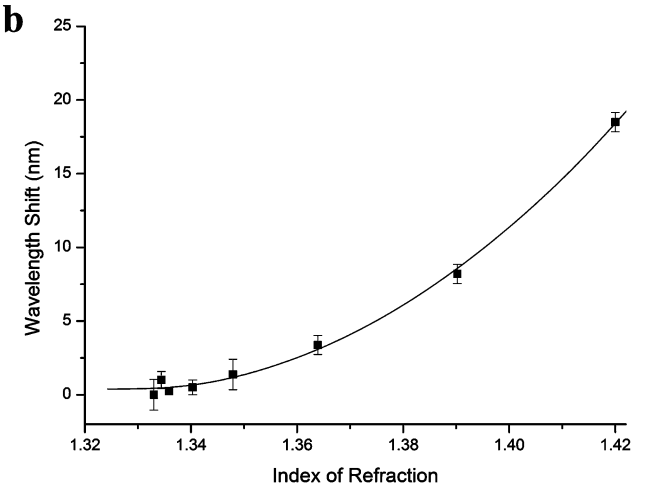

Figure 5. (a) Representative (mean of four replicate samples) transmission spectra for nanohole array (P = 520 nm) in air (−−) and HBS-EP buffer (− − −). (b) Red-shift spectral response to sucrose solution concentration over the range 0% to 50% w/v.

(26) Genet, C.; Ebbesen, T. W. *Nature* **2007**, *445*, 39−46.

(27) Jung, L. S.; Campbell, C. T.; Chinowsky, T. M.; Mar, M. N.; Yee, S. S. *Langmuir* **1998**, *14*, 5636−5648.

A second-order polynomial curve is fitted to the data in Figure 5b ($y = 2140.6x^2 - 5686.4x + 3776.8$, $R^2 = 0.997$) which could be used for calibration purposes. By differentiating this relationship, we obtain wavelength response per refractive index unit (RIU) values of 20.4 nm RIU^{-1} at $n = 1.333$ and 393 nm RIU^{-1} at $n = 1.42$. This finding suggests that increased response could be achieved by binding materials to the surface that possess a high dielectric constant. A previous nanohole study reported a linear response of 333 nm RIU^{-1}.[20] Other substrates yield different responses such as gold nanoshells (328.5 nm RIU^{-1});[28] substrates prepared by nanosphere lithography (191 nm RIU^{-1});[29] and gold colloids (66.5 nm RIU^{-1}).[29] Commercial SPR techniques respond at levels of approximately 2×10^6 nm RIU^{-1}.[27]

Spectral Response to Temperature Gradient. Measurements of bulk refractive index response to temperature over a 16 °C range (24−40 °C) produced a sensitivity of 0.18 nm $°C^{-1}$ or 9 $\times 10^{-4}$ RIU $°C^{-1}$. This initial work, while relevant for determining temperature sensitivity, is limited in comparing biosensor transduction methods since responsiveness in binding interactions is dependent on surface proximity of the plasmon field which varies with different surface structures. Further work will focus on determining the exact relationship between temperature and practical binding responses at the sensor surface to compare nanohole array, LSPR nanoislands and conventional planar SPR formats.

Immunochemical Binding Interactions with Cortisol Linker and Nanoparticle Enhancement. To determine the likely response and dynamic range for the nanohole array system under immunoassay conditions that involve a lower affinity binding interaction (antibody/antigen binding as opposed to the biotin/streptavidin interaction previously studied[20]), the steroid hormone cortisol was used as an immunochemical model compound. Cortisol is an important physiological marker in humans, particularly for the measurement of stress responses.[30,31] The cortisol-OEG-SH compound (Figure 3b) is designed to achieve maximum projection of the steroid into the aqueous mobile phase by use of an oligoethylene glycol linker linked at the 4-position (shown to give maximum antibody recognition in flow-through assays[32,33]). The thiol terminus allows convenient attachment to a gold (or silver) surface by the formation of a dative bond. This compound enables convenient one-step immobilizations without the need to modify intermediate self-assembled monolayers (SAMs). This approach is well suited to inhibition biosensor assays and is particularly well suited for small molecule analysis, that is, for molecules with a molecular weight less than 2000 g mol^{-1} since the conjugation chemistry employed allows optimal presentation of the cortisol for antibody binding thus improving sensor signal by relieving steric obstruction to binding that would otherwise predominate for small molecules and improving antibody capture efficiency.

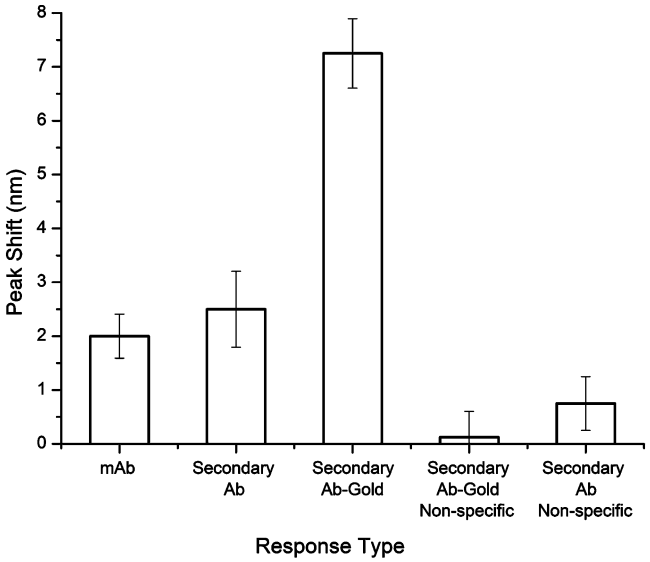

Figure 6. Peak shift for primary antibody (mAb), followed by secondary antibody, and by secondary antibody + gold nanoparticle binding enhancement and, for comparison, the nonspecific binding response of secondary antibody and secondary antibody−gold in the absence of the primary antibody.

Consistent with our bulk refractive index measurements, it was found that with binding tests the (1,1) peak at 780 nm (for a $P =$ 520 nm nanohole array region) is noticeably (3.8 times over the range tested) less sensitive to surface binding events than the (1,0) peak at 1060 nm so the latter was used and monitored to calculate the binding responses. Binding responses for each of the specific and nonspecific binding interactions for monoclonal and secondary antibodies are presented in terms of peak wavelength red shift in Figure 6. The response from mAb binding alone was 2 ± 0.2 nm, which is similar to that determined for the much higher binding affinity biotin−streptavidin binding interaction in a previous study.[20] This result represents a significant improvement in sensitivity since we used a lower protein binding concentration (mAb at 10 μg mL^{-1}) compared to a previous study that used streptavidin (at 250 μg mL^{-1}), smaller sample volumes (2×25 μL compared with 300 μL), a lower affinity binding interaction (K_A of 2.0×10^9 M^{-1} compared with 1×10^{13} M^{-1}) and a larger flow cell volume (30 μL compared with 0.05 μL). The secondary IgG enhanced response cannot be distinguished statistically from that of the primary antibody alone but on average was 0.5 nm higher, indicating little detectable enhancement. The secondary IgG at this high loading predictably gave some nonspecific binding (0.75 nm shift). Enhancement of the mAb response with a secondary IgG−gold conjugate gave a shift of 7.25 nm (a 3-fold enhancement response) demonstrating a much greater shift than with secondary antibody alone for a relatively low affinity binding interaction. This response was in addition to an initial 5.5 nm red shift of the maximum transmission peak upon in situ immobilization, therefore representing a total 13 nm spectral shift. We expect that the 40 nm gold nanoparticles are interacting with the underlying gold layer since they possess a high dielectric constant relative to the buffer solution, and perhaps through cooperative plasmonic effects, giving rise to this larger red-shift in the plasmon peak. It would be of interest to examine the effects of changing gold nanoparticle size and the thickness of the

(28) Sun, Y. G.; Xia, Y. N. *Analyst* **2003**, *128*, 686−691.
(29) Malinsky, M. D.; Kelly, K. L.; Schatz, G. C.; Van Duyne, R. P. *J. Am. Chem. Soc.* **2001**, *123*, 1471−1482.
(30) Summers, C. H.; Winberg, S. *J. Exp. Biol.* **2006**, *209*, 4581−4589.
(31) Southwick, S. M.; Vythilingam, M.; Charney, D. S. *Annu. Rev. Clin. Psychol.* **2005**, *1*, 255−291.
(32) Mitchell, J. S.; Wu, Y.; Main, L.; Cook, C. J. *Anal. Biochem.* **2005**, *343*, 125−135.
(33) Mitchell, J. S.; Wu, Y.; Main, L.; Cook, C. J. *Steroids* **2006**, *71*, 618−631.

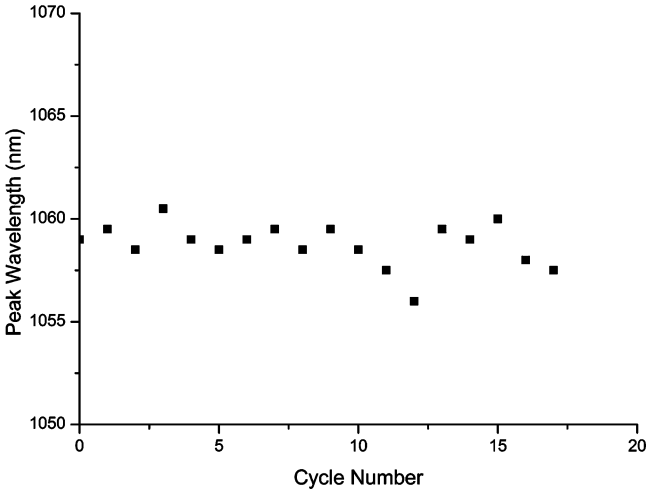

Figure 7. Baseline peak position vs cycle number showing baseline stability after 17 binding and regeneration cycles.

underlying gold on the magnitude of peak shift responses. Nonspecific binding interactions between secondary, and secondary-gold antibodies, in the absence of monoclonal antibody are also shown in Figure 6. Here, it can be seen that there was very low nonspecific binding which further supports the potential for this nanohole array−nanoparticle enhancement system to be used in biosensor assays.

The binding interactions were regenerable, and the surface could last at least 17 binding and regeneration cycles, thus allowing multiple use of a single surface. This is an important capability for an effective plasmonic biosensor and has not been demonstrated before for nanohole systems. The peak position at baseline is plotted vs cycle number in Figure 7. The data show reasonable baseline peak stability. These results indicate that nanohole arrays conjugated with thiol-small molecule derivatives can form the basis of a plasmonic immunobiosensor for the detection of biomolecules. The immobilization and transduction techniques are quite simple to use and offer a route to affordable and portable plasmonic biosensor systems.

CONCLUSIONS

This study has characterized and demonstrated the production of a nanohole array detection system for small molecules using cortisol as the model analyte. Immunochemical binding interactions have been sensed using a new cortisol-linker-thiol derivative for surface modification. This system is fully regenerable and has low nonspecific binding. Gold nanoparticles have been used to greatly enhance the binding response through mass and/or cooperative plasmon effects to achieve a 3-fold wavelength shift over monoclonal antibody binding alone. The system has also demonstrated higher sensitivity in a lower affinity system than those previously studied and is in a regenerable format. This work opens up the possibility of producing low-cost, portable, and robust biosensors for detection of important biomolecules.

ACKNOWLEDGMENT

The authors acknowledge HortResearch Capability funding for this research and access to equipment from the University of Waikato, the University of Canterbury, and the MacDiarmid Institute for Advanced Materials and Nanotechnology. We thank Dr. Yinqiu Wu for useful discussions.

SUPPORTING INFORMATION AVAILABLE

Synthesis of cortisol-OEG-SH derivative. This material is available free of charge via the Internet at http://pubs.acs.org.

Received for review December 17, 2007. Accepted January 21, 2008.

AC702555R